energy&fuels

pubs.acs.org/EF

Article

Sequential Extraction and Characterization of Nitrogen Compounds after Hydrothermal Liquefaction of Sewage Sludge

Joscha Zimmermann, Stefano Chiaberge, Steen B. Iversen, Klaus Raffelt,* and Nicolaus Dahmen

Cite This: *Energy Fuels* 2022, 36, 14292−14303

Read Online

ACCESS | Metrics & More | Article Recommendations | Supporting Information

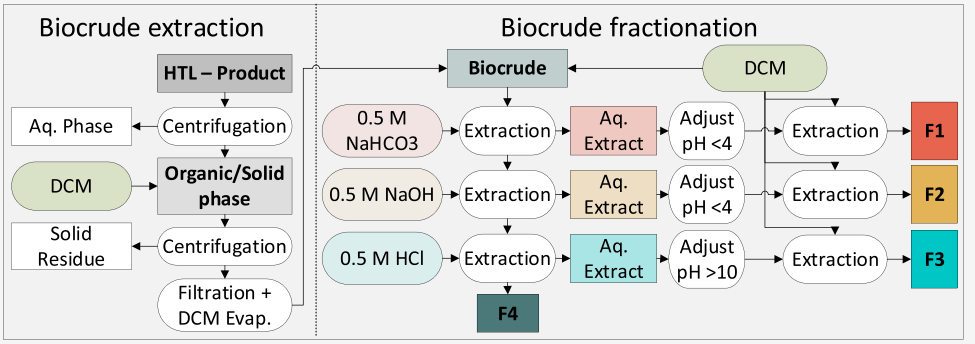

ABSTRACT: Organic solid wastes such as sewage sludge are potential feedstocks for the production of drop-in biofuels. Hydrothermal liquefaction (HTL) is a process that converts the wet sewage sludge into an organic biocrude. To fulfill industrial fuel standards, the considerable heteroatom content of the biocrude needs to be lowered by downstream processes. Nitrogen (N) contained in several compounds poses a challenge and yet, the complex chemical composition of HTL-biocrude samples has hindered detailed analysis and understanding. In particular, N-containing aromatic substances appear very persistent in biocrude. In the present work, two alkaline ($NaHCO_3$ and NaOH) and one acidic (HCL) aqueous solutions were subsequently applied to extract and recover polar N-containing compounds from the biocrude matrix with an N-content of 3.8 wt %. Gas chromatography−mass spectrometry, atmospheric pressure chemical ionization in positive mode, and Fourier transform ion cyclotron resonance mass spectrometry were applied for their characterization and results show that a large share of N-compounds with an aromatic, pyridinic structure was found in the acidic extracted fraction with an N-content of 9.5 wt %. Aliphatic N-compounds were less affected by the separation and ended in the residual fraction. N-compounds with multiple oxygen functionalizations are enriched in the alkaline extracted fractions. This showed that N-compounds with an aromatic structure are strongly affected by polar groups and can potentially be extracted by downstream processes with appropriate solvents.

INTRODUCTION

The desired reduction of CO_2 emissions drives society to identify renewable carbon sources for future liquid fuels and chemicals supply. Also, in order to tackle emerging waste management problems, the valorization of the common waste streams has gained global interest.[1] Sewage sludge is a wet waste stream that contains plenty of valuable organics, such as lipids, carbohydrates, proteins, and inorganic material, often precipitated as phosphor salts.[2,3] In northern European countries, sewage sludge is usually incinerated or disposed in landfills.[4] Otherwise sewage sludge is often used in agriculture, but nowadays it is more and more regulated as pharmaceutical and microplastic residues and pathogens are a concern.[5−7] The method of thermochemical conversion of sewage sludge into energy, gas, or fuel intermediates includes methods of tackling these issues by pyrolysis, gasification, and combustion. One promising conversion process is the hydrothermal liquefaction (HTL). This process uses the beneficial properties of hot, compressed water at elevated temperatures in the range from 250 to 450 °C and pressures above the saturation pressure of up to 350 bar and can convert moisture-rich wet waste biomass such as sewage sludge to a crude oil-like product, named biocrude.[8,9] During the HTL process, biomass-originated polymers decompose into smaller molecules and even pharmaceutical micropollutants and microplastics are decomposed.[10,11]

Due to the often high content of oxygen (18.8−23.5 wt %) and nitrogen (2.5−7.9 wt %) in sewage sludge, the resulting biocrude consists mostly of highly functionalized com-

Received: August 5, 2022
Revised: October 27, 2022
Published: November 16, 2022

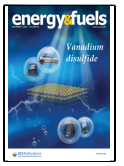

https://doi.org/10.1021/acs.energyfuels.2c02622
Energy Fuels 2022, 36, 14292−14303

pounds.[12] Furthermore, the relatively high lipid content (~20 wt %) is suitable for HTL as they are hydrolyzed into long-chain fatty acids and other derivates such as fatty alcohols are formed.[13,14] Lignocellulosic material (~15 wt %) results primarily in phenolic compounds, cyclic ketones, and short-chain carbonic acids.[15,16] The high protein content in the sewage sludge (~40 wt %) originates from the microbiological processes during wastewater treatment and leads to the formation of nitrogenated compounds.[17−19] Due to the amidation of fatty acids, long-chain amides are formed.[20] Additionally, internal ring closure and Maillard reactions build up aromatic heterocycles based on pyrrolic or pyridinic ring structures.[21]

The direct use of biocrude as a drop-in transportation fuel is limited, as the distillation cut requirements are often not fulfilled due to the high contents of nitrogen and oxygen. Therefore, an extensive upgrading step is required, which would include primarily a catalytic hydrotreating process.[22,23] Because the biocrude contains a large share of nitrogen-functionalized compounds, often bound in an aromatic ring, high hydrogen partial pressure and relatively high reaction temperatures are needed.[24] Double bonds in the aromatic ring need to be saturated and eventually cracked to remove nitrogen, which results in higher hydrogen consumption. Furthermore, it is believed that N-heteroaromatic compounds can form organometallic complexes, likewise as they appear in nature as porphyrin or heme.[25,26] This transfer of inorganic species into the hydrotreating process can lead to irreversible catalyst fouling and plugging.[27] Haider et al.[28] assume that these organometallic compounds led to an increased coke formation. They show often surface-active properties and are assumed to cause the formation of emulsions, which results in difficult product phase separation after the HTL process.[29] Many of the N-compounds derived from the HTL are chemicals of interest to the industry.[2] Numerous research studies have focused on the production of valuable chemical N-compounds derived by the HTL of biomass, agreeing it is a challenge to produce specifically value-added nitrogen-containing compounds, due to the complex composition of the starting biomass.[30] The subsequent separation of N-compounds is therefore of interest, as it happened when the generated biocrude is separated from the aqueous byproducts. Ekpo et al.[31] identified a strong influence of the pH of the aqueous phase on the recovery of nitrogen whereas Chen et al.[32] extracted emulsified N-compound in water. Fonts et al.[33] recovered a comparable bio-oil derived by pyrolysis of sewage sludge-added compounds by applying organic and inorganic solvents for fractionation. Nevertheless, to effectively evaluate HTL-biocrude as a potential source of drop-in fuels and to design an appropriate downstream upgrading process, a full characterization of the biocrude-containing compounds is needed.

For the characterization of biocrude composition, commonly gas chromatography (GC) coupled with mass spectrometry (MS) is used. GC is limited to volatile compounds with lower molecular weight and the conventional MS systems are not able to resolve and identify hundreds of components found in a single analyte as they lack sufficient resolution and mass accuracy.[34] This makes the use of pre-chromatographic separation necessary, reducing the complexity of the product composition. Bio-oils derived from biomass pyrolysis or HTL contain large quantities of polar substances, which would make the results non-comparable. Therefore, specified methods and the use of modified solvent systems are applied.[35−37] Aqueous solutions at different pH values were used in several studies to separate organic compounds by different polarity. Boocock et al.[38] separated oxygen-rich HTL oil derived from aspen wood, whereas Dote et al.[39] and Das et al.[40] applied this acid−base separation method on bio-oil derived from nitrogen-rich biomass feedstocks. New, advanced analytical systems try to unravel the complexity of the biocrude composition with high mass resolving power and mass accuracy, as provided by Fourier transform ion cyclotron resonance MS (FTICR MS) or other high-resolution MS systems.

This work aims to separate N-compounds from the complex HTL-biocrude matrix, produced from sewage sludge in a state-of-the-art continuous pilot process. In a first step, the biocrude is separated sequentially into four fractions by applying two alkaline and one acidic aqueous solutions. The mass balances and the recovery of carbon and nitrogen are carefully determined. In the following step, the chemical composition of the fractions is analyzed by conventional GC−MS and the most abundant N-compounds are identified. With a focus on N-heteroatom classes, their distribution and the double bond equivalent (DBE) were determined by FTICR MS and discussed with preceding results, providing information on functionalization, aromaticity, and structure. That way, the fate of specific N-compounds after treatment with aqueous polar solutions can be determined. Furthermore, a qualitative statement can be given to plan for further downstream processing and the potential to recover or remove the process valuable and harming organic components, respectively.

MATERIALS AND METHODS

All chemicals used for the experiments were obtained of analytical grade and obtained from Merck (MilliporeSigma).

Biocrude Production. The HTL-biocrude sample used in this study was produced at the Pilot and Test Facility in Aalborg, DK. The production campaign in 2019, processed 500 kg of sewage-containing slurry, within the NextGenRoadFuel-Horizon2020 project, which aims to develop an effective technology pathway to valorize the combination of sewage sludge, food waste, and construction wood residues as sustainable drop-in fuels. For this purpose, non-digested sewage sludge in dewatered form (24.9 wt % dry matter) was collected from a wastewater treatment plant located in Farsø, Denmark. A pumpable slurry containing 21 wt % sewage sludge (dry matter), 2.5 wt % sodium hydroxide, and 2.5 wt % potassium carbonate was prepared by mixing the ingredients and diluting them with distilled water to the given concentrations. The slurry was processed at a flow rate of around 30 kg/h and converted at 400 °C and 320 bar above the critical point of water. A mixed emulsion-like liquid product consisting of aqueous, oil, and solid phases was degassed at 60−80 °C and slight overpressure and collected for this study. The collected sample was kept in a 1 L borosilicate bottle and stored in the fridge and subsequent experiments were conducted in early 2020.

Extraction of Oil from HTL Product. The as-received HTL product must be separated into an organic biocrude, aqueous, and solid phases. Afterward, the proposed sequential extraction methodology could be applied to the biocrude phase. In a first step, 50 g of HTL product emulsion was separated into aqueous and organic/solid phases by centrifugation at 7000 rpm (Eppendorf EP 5430). The received aqueous supernatant was discharged whereas the precipitate was mixed with 40 mL dichloromethane (DCM), vortexed for 2 min and subsequently centrifuged again with 7000 rpm. The DCM supernatant was filtered through a 0.45 μm nylon filter (GE Whatman) and evaporated overnight under a gentle nitrogen stream.

Sequential Extraction. The extraction procedure to separate polar compounds follows a modified procedure, proposed by Boocock

https://doi.org/10.1021/acs.energyfuels.2c02622
Energy Fuels 2022, 36, 14292−14303

et al.[38] Following a sequential extraction with aqueous solutions of sodium bicarbonate ($NaHCO_3$), sodium hydroxide (NaOH), and hydrochloric acid (HCl). The aqueous extracts were re-extracted with DCM after titration of the aqueous solution to a contrary acidic or alkaline pH. Dissociated organic compounds that are soluble in polar solutions before would be protonated or de-protonated into their non-polar form. An appropriate non-polar solvent could re-extract these compounds. This procedure results in four fractions, fraction F1 and fraction F2 recovered from alkaline agents, fraction F3 recovered from an acidic agent, and the residual fraction F4.

In detail, 5 g of biocrude was mixed in 100 mL DCM and transferred to a separatory funnel filled up with 50 mL of a 0.5 mol·L^{-1} solution of $NaHCO_3$. The mixture was shaken vigorously for 5 min and was allowed 1 h for phase separation. The bottom DCM phase was transferred to a fresh separatory funnel, including the emulsion layer (see Supporting Information, S1) at the phase boundary. The aqueous supernatant was collected in a beaker and the funnel was washed with 2 mL of DCM, which was added to the second funnel. This procedure was repeated two times with 25 mL of the $NaHCO_3$ solution and two times with 25 mL of deionized water. All aqueous samples were combined in one 400 mL beaker. Next, the DCM phase was extracted by a similar procedure with 0.5 mol·L^{-1} NaOH and with 0.5 mol·L^{-1} HCl, including the same deionized water washing steps. The two collected aqueous alkaline solutions were titrated with 10 mol·L^{-1} HCl solution to a pH of below 4, and the aqueous acidic solution with 10 mol·L^{-1} NaOH to a pH above 9. Then, each combined solution was transferred from the beaker again to a separatory funnel. Beakers were washed with small amounts of DCM to add precipitated organics to the funnel. The three solutions were re-extracted with the same procedure as described above with 50 mL and two times with 25 mL of DCM. Each extract was filtered through a 0.45 μm nylon filter to remove suspended solids. To yield a solvent-free biocrude, DCM was evaporated under a gentle nitrogen stream overnight.

Characterization of Organic Fractions. The carbon (C), hydrogen (H), nitrogen (N), and sulfur (S) contents of the biocrude samples, as well as solid products, were analyzed using a CHNS analyzer (Vario EL cube, Elementar Analysentechnik GmbH, Hanau, Germany). The oxygen (O) content was determined subsequently by difference.

The extracts were analyzed by a gas chromatograph (Agilent 6890N, Santa Clara, CA, USA) coupled with a mass spectrometric detector (MSD, Agilent 5973N, Santa Clara, CA, USA) on a Rxi-5MS column with a 30 m × 0.32 mm diameter and a film thickness of 0.25 μm (Restek Corporation, Bellefonte, PA, USA). About 10 mg of samples were prepared in 0.5 mL of chloroform, 0.5 μL of which were injected at 280 °C in 1:20 split mode, using helium as the carrier gas (1.5 mL·min^{-1}). The GC oven program started at 70 °C which was held for 2 min and progressed at 8 °C·min^{-1} to 180 °C and at 4 °C·min^{-1} to 280 °C, followed by a holding time of 15 min. The MSD was operated in 70 eV EI mode with a source temperature of 230 °C and a solvent delay of 4.8 min, followed by scanning from 35 to 500 m/z with a frequency of 3.9 scans per second.

Biocrude and recovered fractions, F1 to F4, were analyzed by atmospheric pressure chemical ionization (APCI) in positive ion mode (+) by using a 7 T FTICR (LTQ-FT Ultra Thermo Scientific) MS analyzer. These samples were diluted in $CHCl_3$/acetonitrile 1:1 and infused at a flow rate of 100 μL·min^{-1} by a syringe pump into the APCI ion source. The final concentration of the solution in the APCI ion source was around 0.4−0.6 mg·mL^{-1}; typical APCI (+) conditions were as follows: source heater, 380 °C; source voltage, 5 kV; capillary voltage, 7 V; tube lens voltage, 60 V; capillary temperature at 275 °C; sheath gas, 60 arbitrary units; and auxiliary gas, 10 arbitrary units. The mass spectra were acquired in positive mode with a mass range of m/z 100−1000. The resolution was set to 200,000 (at m/z 400). 360 scans were acquired for each analysis to improve the signal-to-noise ratio using the Booster Elite system (Spectroswiss, Lausanne, Switzerland), which allowed to register directly the transient data. Transients were then processed by Peak-by-Peak-Petroleomic software (Spectroswiss, Lausanne, Switzerland). The 360 transients were first averaged and then FT was applied to obtain a single averaged mass spectrum. The resulting spectrum was further processed to remove the noise (thresholding set to 6 Sigma of the background noise) and internally recalibrated through the unwrapping method.[41]

Data Analysis and Visualization. Data generated by GC−MS were analyzed with Agilent's MassHunter quantitative analysis software (unknown analysis) v.10.1 (Agilent, Santa Clara, CA, USA). The compounds were identified by Agilent's deconvolution algorithm and the NIST 2017 library, proposed compounds with a score above 80 were considered as a match. If multiple compounds fulfilled this score, as it often occurred specifically for long-chain aliphatics, the decision was based on chain length, retention time, and alignment with our in-house database. The relative peak area of an identified compound was based on the total-ion-current chromatogram, provided by the software.

The FTICR MS generated data were analyzed with Peak-by-Peak-Petroleomic software. Around 6000−8000 different peaks were obtained in each single mass spectrum. The composition constraints used for the composing function were C: 7−80, H: 12−150, N: 0−4; O: 0−4; 13C 0−1. The final attribution of these peaks was obtained using the composing function of Peak-by-Peak with the error limit of ±2 ppm. The software allows internal recalibration of the mass spectra (using known compounds or internal standards), reducing remarkably the associated errors of less than 1 ppm. The classes were determined through the spectral slice function. An example is attached for the class O1N1 with a wide tolerance of ±500 ppm as shown in Supporting Information, S6, showing the different slices related to different classes and with the set limit of ±2 ppm used in our approach.

Considering the composition constraints and the statistical distribution of ions in each class (Gaussian-like distributions similar to those found for crude oil samples), the multiple matches for a single ion can occur only at high m/z values (the slice distributions widen over m/z 500). At such high values of m/z, the ion intensities were found to be lower; therefore, we believe that the risk of wrong assignment would not impact the overall characterization of the sample.

The molecular formulas were categorized according to different parameters, such as the number of heteroatoms (N, O, and S) and the degree of saturation expressed as DBE. DBE values were calculated based on the molecular formula $C_cH_hN_nO_oS_s$, according to the following equation

$$\mathrm{DBE} = c + 1 - \frac{h}{2} + \frac{n}{2}$$

Specific classes of species were determined according to the heteroatoms present, and their relative abundances were used for deriving class distribution plots. The most abundant classes were then visualized in DBE versus carbon number (Cn) plots according to their carbon number, DBE value, and relative abundance in the mass spectrum using a color code.

The predicted empirical formulas were searched within the ChemSpider database to identify possible structures.[42] The proposed structures from the database were compared with compounds identified by previous GC−MS analysis or checked with the literature on HTL-biocrude analysis.

For data processing and plotting the Python libraries, NumPy, Pandas, and Matplotlib were used. Principal component analysis (PCA) was performed with the scikit-learn package within Python. The sums of relative abundances for each heteroatomic class were scaled and used as input variables for PCA. Chemical structures were drawn with ChemDraw Professional 10.1 (PerkinElmer, MA, USA).

RESULT AND DISCUSSION

Elemental Analysis of HTL-Biocrude Extracts and Corresponding Yields. The elemental composition of the biocrude and the received extracts, F1, F2, F3, and F4, based on dry basis, as well the H/C and N/C ratios and extraction

https://doi.org/10.1021/acs.energyfuels.2c02622
Energy Fuels 2022, 36, 14292−14303

Table 1. Biocrude and Extract Yields and Composition[a]

	dimension	biocrude	fraction 1	fraction 2	fraction 3	fraction 4	petroleum[44]
C	wt %	76.0	74.7 (1.0)	74.0 (0.7)	73.8 (0.4)	75.8 (0.1)	83−87
H	wt %	11.0	11.0 (0.7)	11.4 (0.9)	9.2 (0.2)	11.7 (0.0)	10−14
N	wt %	3.8	3.0 (0.4)	1.9 (0.3)	9.5 (0.5)	3.5 (0.3)	0.1−2
S	wt %	1.0	0.8 (0.1)	0.7 (0.3)	0.7 (0.2)	0.7 (0.0)	0.05−6
O[b]	wt %	8.2	10.4 (1.8)	12.1 (1.2)	6.8 (0.4)	8.4 (0.3)	0.05−1.5
H/C	mol H/mol C	1.74	1.77	1.84	1.49	1.86	1.38−2.02
N/C	mol N/mol C	0.04	0.03	0.02	0.11	0.04	0.00−0.02
extraction yield[c]	wt %		11.0 (0.9)	13.6 (1.3)	5.2 (0.9)	54.3 (3.2)	

[a]The number in parenthesis shows the standard deviation of the mean. [b]Is calculated by difference. [c]Based on the biocrude extract.

yields is compiled in Table 1. The elemental composition of the biocrude is in agreement with products obtained from continuous HTL of sewage sludge, referred by Jarvis et al.[34] and Haider et al.[43] To compare the samples with petroleum, the average elemental composition provided by Speight[44] is added to the table. It is visible that biocrude and the extracted fractions show a lower C- and H-content, than the referenced petroleum. Furthermore, all fractions show also lower C-contents than the biocrude. This could be related to the precipitation of not-analyzed, surface-active carbonaceous material during the extraction procedure, which is shown in Supporting Information, S1. Petroleum crude is usually characterized by a low heteroatom N- and O-content, which differs largely from the biocrude and extracted samples. The N-content is slightly lower than that in the original fractions 1, 2, and 4, with no significant effect. Otherwise, F3 shows a substantially higher value. Contrary to the N-content, the O-content is lower in F3. Analyzing the H/C ratios and comparing the original biocrude with its extracts and petroleum, it can be noted that F2 and F4 show increased values close to the higher range petroleum ratios. This is a strong indication of an accumulation of aliphatic structures with O- or N-functionalization. F3 shows a relatively low H/C ratio, close to a bituminous fraction.[44]

Concerning the C- and N-recoveries as shown in Figure 1, an accumulated recovery of 83.2 ± 6.2% of C and 77.7 ± 9.5% of N could be archived. Most C and N are recovered in F4. For the ratio between N- and C-recovery, F3 shows by far the highest value with about 2.56, whereas F1 and F4 do not differ significantly with values of 0.8 and 0.91, respectively, and F2 shows the lowest ratio with 0.51.

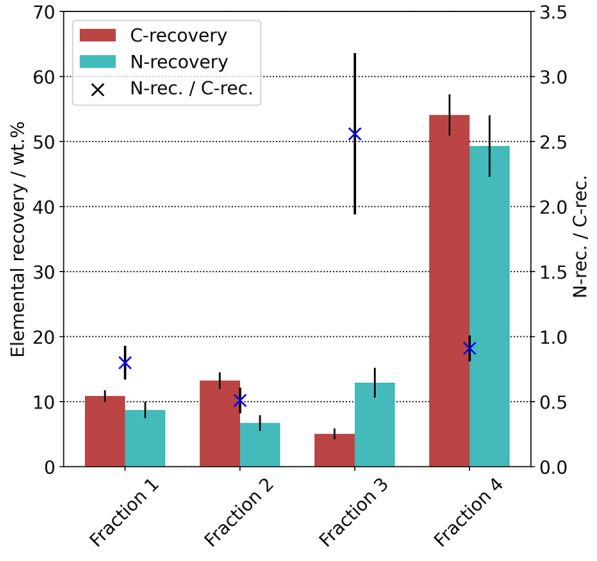

Figure 1. Elemental recovery and ratio of biocrude extracts.

Gas Chromatography−Mass Spectrometry. The identification of volatile compounds in the extracted fractions was carried out by GC−MS. The 20 most abundant peaks and their resulting compounds are classified by their functionalization into six groups and the relative peak areas of the total-ion-current chromatogram of each identified compound are summed up. The occurrence of these groups in the biocrude and the different fractions is shown in Figure 2. The related chromatograms of each fraction are shown in Supporting Information, S2 and the identified compounds are listed in Supporting Information, S3.

Within the biocrude, non-polar compounds with different O- and N- functionalizations are identified, which accumulated in the following extracted fractions F1, F2, F3, and residual F4. The main compounds identified in F1 are O-containing aliphatic structures functionalized by a carboxyl group such as fatty acids. The relative area of this compound group amounts to 91.2% of the identified signals. In addition, a small proportion of 8.8% of the identified compounds are O-containing aromatics such as phenols, possibly branched with methyl groups. Both, carboxyl and phenol groups are found as well in F2 with a relative area of 31 and 60.1%, respectively. A small share of the peaks can be allocated to N-functionalized groups with aliphatic compounds such as amides and with aromatic compounds with a pyrrole group such as indole derivates. All of the identified compounds in F3 contain N-heteroaromatic structures consisting of either pyridine or a pyrrole functional group with a relative peak area share of 60.5, and 39.5%, respectively. It should be noted that the pyrrole functional groups may also contain a pyridine group, for example, in the form of pyridoindoles. Compounds containing pyridine-functionalized compounds were exclusively found in F3 by GC−MS analysis. The residual fraction F4 shows a large share of 54.8% of the relative peak area of identified compounds which are related to aliphatic compounds with hydroxyl or carbonyl groups. The most dominant compounds here are fatty acid alcohols as well as sterol derivates. An additional 19.2 and 17.9% of the identified compounds account for aliphatic amides (fatty acid amides) and heteroaromatic pyrrole (indoles) groups. Non-polar compounds found in this fraction reach a share of 8.1%.

Although a large variety of compounds were identified by GC−MS, the poor resolution of peaks does not allow the determination of organic compounds present in lower abundances. This does occur especially for N-heteroaromatic compounds, as these are present in a wide variety of different derivates. Additionally, the compounds of higher molecular

https://doi.org/10.1021/acs.energyfuels.2c02622
Energy Fuels 2022, 36, 14292−14303

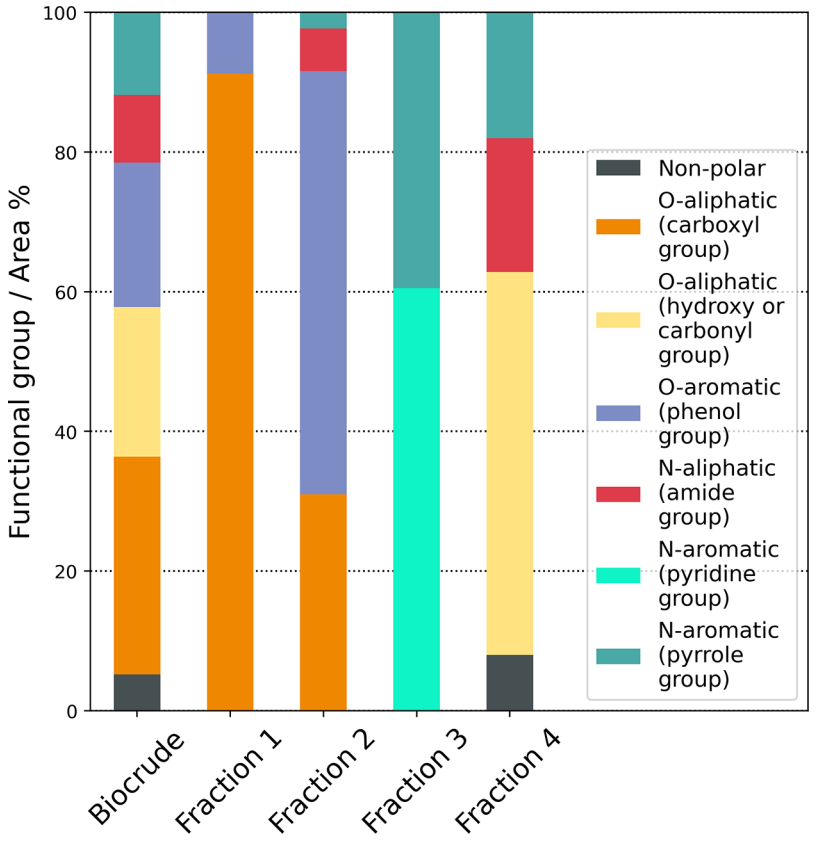

Figure 2. GC−MS results of the most abundant compounds in the extracted fractions (F1 to F4) given in area percentage.

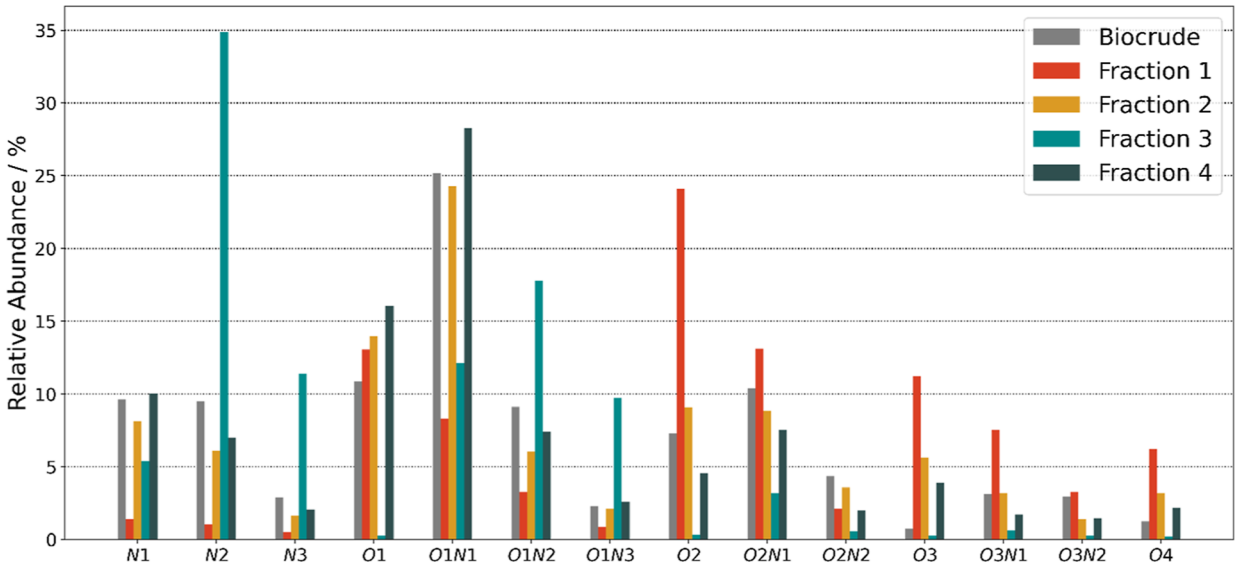

Figure 3. Heteroatom distribution (molar heteroatom content) of selected classes in the biocrude and extracted fractions F1−4.

weight and larger polarity are eluted slowly from the GC column, resulting in an even lower resolution. For this reason, a high-resolution MS technique was applied.

Fourier Transform Ion Cyclotron Resonance Mass Spectrometry. To get an even more detailed characterization of N-containing species in the three fractions obtained from extraction, a Petroleomic approach was employed. Common soft ionization techniques such as APPI, electrospray ionization, and APCI in positive ion mode are especially suitable for proton-accepting functionalized groups such as amines or pyridines. As N-heteroaromatic species also appear in pyrrolic forms (pyrrole, indole, and carbazole derivates), which are not strong proton acceptors, therefore, APCI seems to be the most suitable ionization technique and was applied in this study too.[45,46] Negative ion modes are suitable for hydrogen-donating compounds as they are primarily found in O-heteroatom-containing substances. Phenols are an example of this and are assumed to be largely underestimated with the ion source conditions employed, as they are not effectively

https://doi.org/10.1021/acs.energyfuels.2c02622
Energy Fuels 2022, 36, 14292−14303

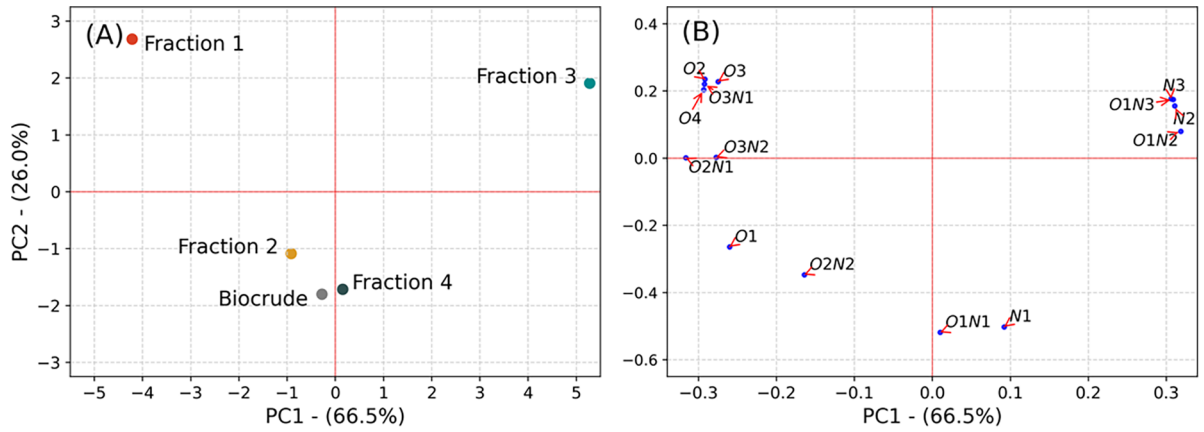

Figure 4. (A) Scoring plot and (B) loading plot from PCA of the relative abundances of heteroatom classes in the biocrude and extracted fractions F1−4.

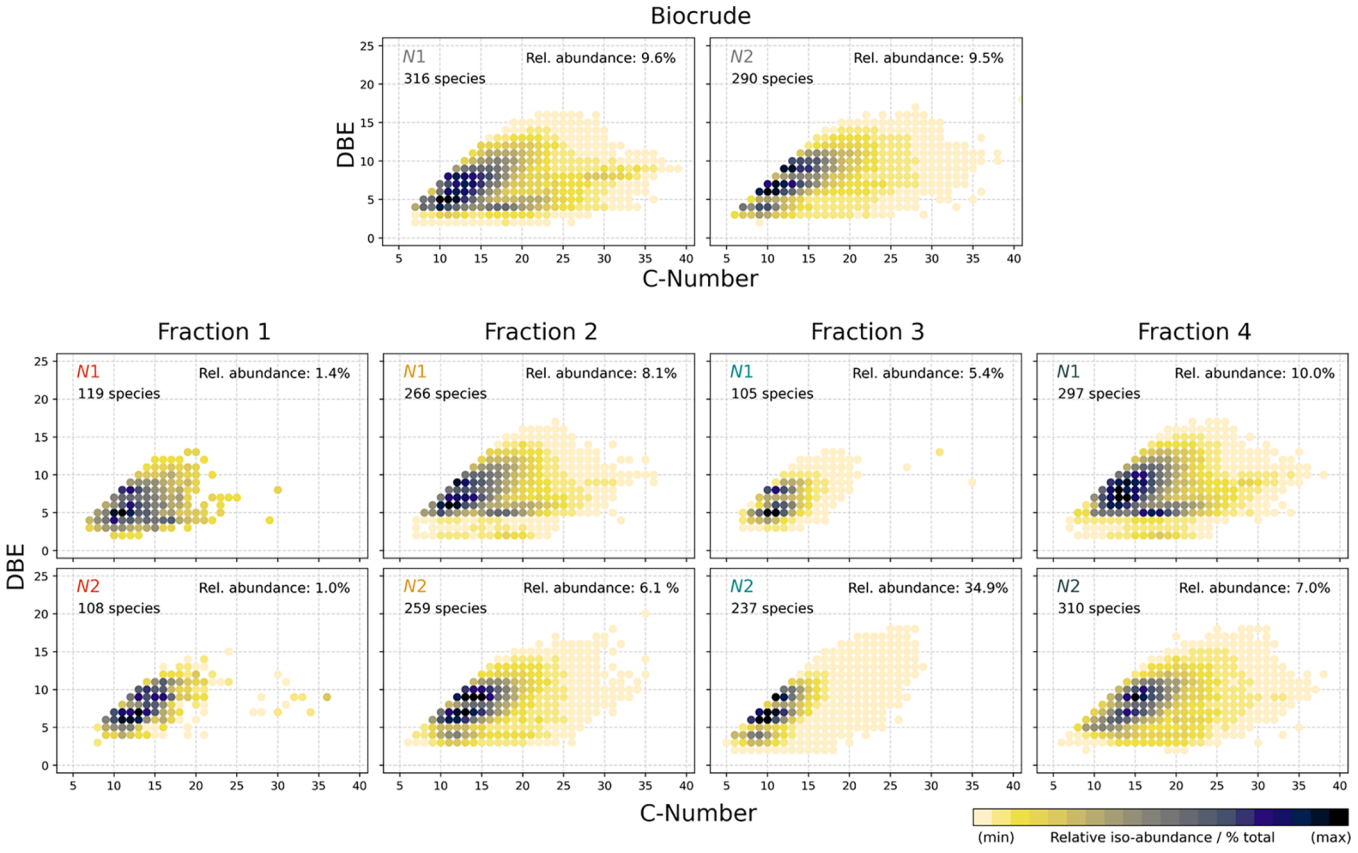

Figure 5. Relative intensity scatter plots of Cn vs DBE distribution of the classes N1 and N2 of the extracted fractions.

ionized.[46] Therefore, in the following section, the discussion on the O-functionalized group is a more qualitative one.

Heteroatom Class Distribution. The heteroatom class distribution determined from positive APCI mode FTICR MS of the four extracted fractions is shown in Figure 3. The results can be divided into 14 classes, denoted by the number of N- and O-atoms in a given compound (N1, N2, N3, O1, O1N1, O1N2, O1N3, O2, O2N1, O2N2, O3, O3N1, O3N2, and O4). It needs to be noted that the results are given in relative abundances in each class. Thus, no information on absolute content is provided.

In F1, high abundances of oxygenated species can be identified in graduating order of O2 (24.1%), O2N1 (13.0%), and O1 (13.1%). The three most abundant classes in F2 are oxygenated as well, namely O1N1 (24.3%), O1 (14.0%), and O2 (9.1%). The third fraction F3 shows high abundances for classes containing predominantly multiple nitrogen atoms such as N2 (34.9%), O1N2 (17.8%), and N3 (12.1%). The residual fraction F4 is nearly identical in heteroatom distribution to F2, in the order of the class O1N1 (28.3%), O1 (16.1%), and N1 (10.0%) as the most abundant ones.

To identify relations and differences between the extracted fractions based on the abundance of heteroatomic classes, an explorative PCA was applied. PCA is used for exploratory data analysis, reducing the 14 input variables of the relative abundances for each heteroatomic class into principal

https://doi.org/10.1021/acs.energyfuels.2c02622
Energy Fuels 2022, 36, 14292−14303

components. The two principal components (PC1 and PC2) are able to describe 92.5% of the total explainable variance. The score plot of PC1 versus PC2 is shown in Figure 4A. PC1 accounts for a variance of 66.5% and shows large differences between alkaline extracted F1 (PC1 value of −4.2) and the acid extracted F3 (PC1 value of 5.3). F2 has a negative PC1 value of −0.9 and shows proximity to F4 with a value of 0.1. The starting material biocrude shows a PC1 value of −0.2. To identify the orientation of specific classes, the loadings, responsible for PC1 and PC2, are analyzed and plotted in Figure 4B. PC1 is strongly moved into a negative value by oxygenated classes on the left, namely O2−4, O2N1, and O3N1−2. Multi-nitrogenated classes such as N2−3 and O1N2−3 are orientated on the right and affect PC1 to positive values. This match the presence of O-functionalized groups such as carboxylic acids from previous GC−MS analysis. This suggests that the donation of protons governs the trend of PC1 to the left. Contrary to the acceptance of a proton, the basic character of N in the form of pyridine and amine compounds governs the trend along PC1 to the right. This is again in agreement with the previous GC−MS results of F3. The classes N1, O1N1, O1, and O2N2 are orientated close to the center along PC1 and can be considered to be less affected by acids and bases. Matching compounds to these four classes were again found by GC−MS, predominantly in F2 and F4. Furthermore, these classes are responsible for negative PC2 values, whereas multi-heteroatom classes with a higher degree of functionalization weigh PC2 into positive values. F1 and F3 show positive PC2 values of 2.7 and 1.9, respectively. Biocrude, F2, and F4 have negative values of −1.8, −1.1, and −1.72, respectively. It can be observed that these three fractions are clustering, indicating small differences in terms of their heteroatom class distribution.

Compositional Space of Specific Heteroatom Classes. The composition of the most abundant N-containing classes found in the extracted fractions is explored in relative intensity scatter plots of Cn versus DBE. These plots are class-specific and give additional information about the primary compounds present in each fraction. With the information of the Cn and DBE values, the base structure of a species can be determined. Lower DBE values between 1 and 3 suggest the presence of aliphatics, whereas higher values above 4, especially with low Cn, are probably related to condensed, aromatic structures. In addition, Cn provides information about the degree of alkylation of a certain species. A higher Cn suggests the alkylation of the base structure with longer or multiple alkyl chains. In addition, the dominant O-containing classes O1 and O2 are shown for qualitative purposes in the Supporting Information. In the following, the DBE versus Cn plots for different classes of substances are presented and discussed.

N*x*-Classes. The classes functionalized exclusively with nitrogen, N1 and N2, are shown within their relative intensity scatter plots in Figure 5. The molecular structures of the discussed substances are depicted in Figure 6.

The N1 class in the biocrude shows a relative abundance of 9.6% including 216 species. F1 shows a low relative abundance with 1.4%, including 119 species with the highest intensity are identified with a DBE of 4 and a Cn of 10. Suggested structures are depicted in Figure 6. As a certain acidity is expected from compounds in this fraction, it is suggested, that these species are related to tetrahydro-indole structures instead of pyridines. Similar compounds are found within the species of the N1 class in F2 and F4, but with a much lower intensity. For both

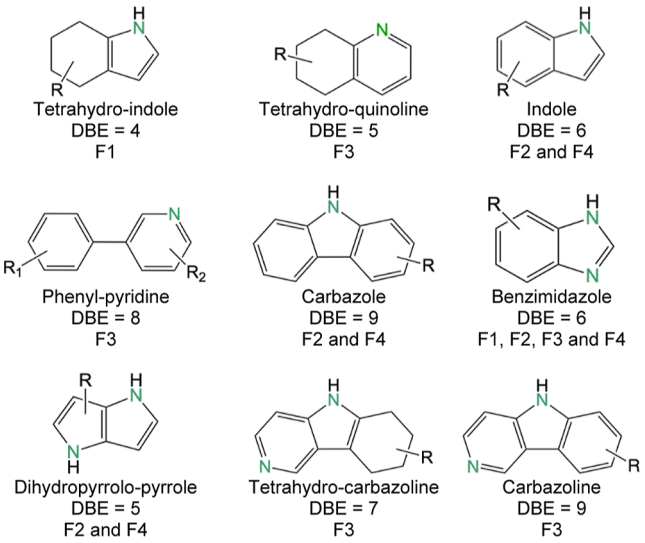

Figure 6. Suggested N1 and N2 species within the extracted fractions.

these fractions, this class represents 8.0 and 8.4% of all 266 and 297 identified species, respectively. In addition, both fractions show high intensities within an area between a DBE of 6−10 and a Cn of 10−16, suggesting alkylated N-heteroaromatic structures.[45] In F2, the highest intensities are identified at a DBE of 6 and 9 and a Cn of 10−13. Different indole and carbazole derivates were identified by GC−MS and have a corresponding DBE, suggesting the presence of more such compounds in this fraction, with more or higher alkyl chains. In F4, the highest intensities seem to concentrate at a DBE of 7 and 8 and a Cn of 13−14. These values hint at tetrahydro-carbazol and dihydro-carbazole compounds. Due to the overall higher Cn in F3, a higher alkylation than in F2 can be assumed. Long-chain aliphatic species are found with relatively low intensity at a DBE of 2 and a Cn between 16 and 18, in the form of nitriles. These compounds are formed by amidation and subsequent dehydration of fatty acids.[47] Considering the orientation along PC1 in the previous PCA, N1 species in F2 and F4 tend to show light acidic/non-polar characteristics which applies to the before described structures.[48] The relative abundance of the N1 class of F3 is given with 5.4% comprising 105 species and is therefore relatively low considering the fact that this fraction contains the highest N-content of all fractions. The highest intensities within this class are located at a DBE of 5 and 8 and a Cn of 10−12. The orientation of PC1 suggests the appearance of basic N-compounds, which can accept protons. The identified compounds by GC−MS, referring to such DBE values are derivates of tetrahydro-quinoline and phenyl-pyridine. More such compounds are suggested in this fraction with a higher degree of alkylation. The basicity of N in these compounds was analyzed and described in comparable extracts with similar species by Zaki et al.[49] and Cao et al.[50] on N-rich HTL-biocrude from spirulina and pyrolysis oil from sewage sludge. As the compositional space of F3 is starting from a DBE value of 4, it is suggested that no alkaline primary or secondary amines are present in sewage sludge biocrude. Within the N1 class, notable differences between the biocrude and F4 within the compositional space are missing. The relative abundance is slightly increasing, and the identified species are more or less in the same range. This is in line with the observations made by PCA, where a clustering of these two fractions is observed.

https://doi.org/10.1021/acs.energyfuels.2c02622
Energy Fuels 2022, 36, 14292−14303

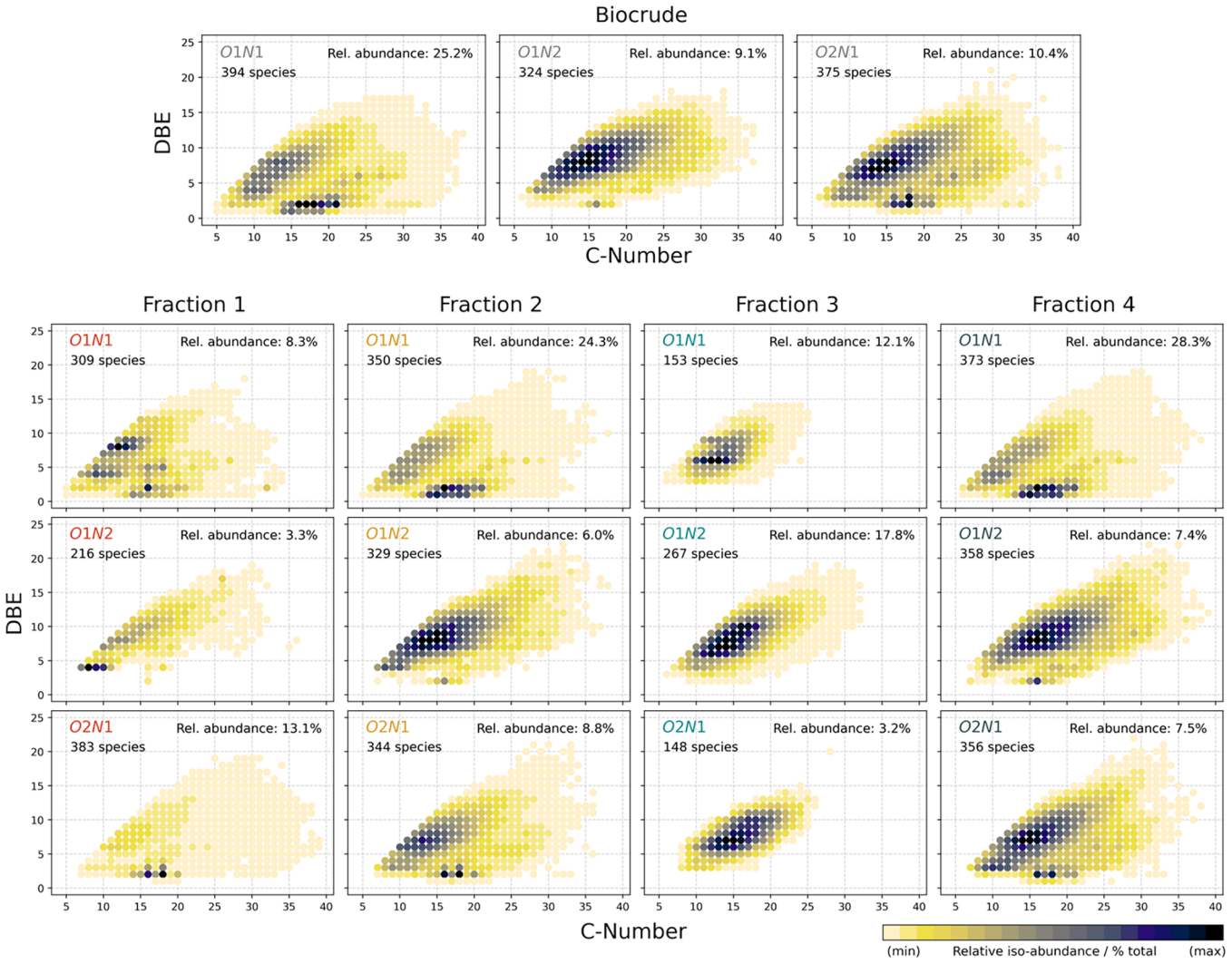

Figure 7. Relative intensity scatter plots of Cn vs DBE distribution of the classes O*x*N*x* of the extracted fractions.

The N2 class within the biocrude is showing a relative abundance of 9.5% over a 290 species. Within F1, an even lower relative abundance of 1.0% over 108 compounds is given. The highest intensities are found at a DBE of 6 and a Cn of 11−13. Similar species showed high intensities in F2 and F3. Other than the N1 class, F2 and F3 show comparable compositional spaces within their relative intensity scatter plots. The N2 class shows in F2 a relative abundance of 6.1% over a range of 259 species. In F3, this class shows an extraordinary high relative abundance of 34.4%, covered by 237 species. In both of these fractions, the highest intensities are located at a DBE of 6, 7, 9, and 10. In F2, the Cn of these species are 11−15, whereas in F3 the Cn is lower with a value between 9 and 11. These species are suggested to refer to benzimidazole or azaindole derivates at a DBE of 6 or also in combination with an added benzene ring, carbazoline derivates at a DBE of 9 are also identified by GC−MS analysis.[48] The appearance of these compounds in F2, F3, and even in small amounts in F1, can be explained by the amphoteric character able to act as weak acids and bases.[51] Furthermore, strong basic species are suggested to be present in F3, such as bipyridines, naphthyridine, and quinazoline, with a degree of aliphatic alkylation and addition of benzene rings. The relative abundance of the N_2 class in F4 with about 7% is spread over a wide range of 311 species, again located in the aromatic area with a DBE of 6−9 and a Cn of 13−16. The extensive variation in Cn for any given DBE value and the high count of detected species with 311, indicates a large degree of alkylation, which is related to the low polarity of this fraction. These compounds can be related to carbazole derivates and species that could be based on the structures of benzopyrazines and dihydropyrrolopyrroles, which are common Maillard reaction products or possible melanoid fragments.[52,53] Within the N2 class, the relative abundance is decreasing from the biocrude to F4, which can be referred to the string accumulation of such species in F3. The previously described structures of the N1 and N2 class are schematized in Figure 6. The abbreviation "R" within the chemical structure is representing different alkyl chain residues. In addition, the DBE value and the suggested fraction are highlighted.

O*x*N*x*-Classes. The relative intensity scatter plots of classes functionalized with N and O, namely O1N1, O1N2, and O2N1 are shown in Figure 7. The molecular structures of the discussed substances are depicted in Figure 8.

The O1N1 class shows a relative abundance of F1 of 8.3% with a range of 309 species. The highest intensity is located at a DBE of 2 and a Cn of 16, which can be related to C16 fatty acid amide. Further, the abundances at a DBE of 8 and a Cn of

https://doi.org/10.1021/acs.energyfuels.2c02622
Energy Fuels 2022, 36, 14292−14303

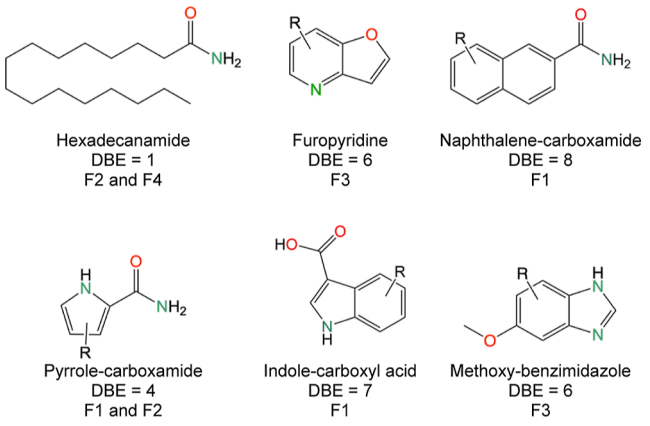

Figure 8. Suggested O*x*N*x* species within the extracted fractions.

12 and 13 stand out. These species are suggested to be composed of short-chain aliphatic amides, connected to a naphthalene structure, as latter is able to donate a proton. F2 and F4 show similarities within their compositional space. The relative abundances of this O1N1 class are given in both fractions with high values of 24.3 and 28.3% with a large variety of 350 and 373 species, respectively. The highest intensities are located in the aliphatic area with a DBE of 1 and 2 at Cn values between 16 and 18; they can be related to fatty acid amides which are common amidation products of fatty acids and amines during the HTL process.[20] F3 shows a relative abundance of 12.1% of O1N1 species with a comparatively low number of 151 species. The intensities are highest at a DBE of 6 and a Cn between 10 and 14. These can be associated with basic pyridine structures in addition to a furan ring, namely furopyridines. Similar compounds are assumed to appear in HTL-biocrude from sewage sludge as well as shale oil samples.[48,54]

The 216 species within the O1N2 classes in F1 results in a relative abundance of 3.3%. The highest intensities of species are located at a DBE of 4 and a Cn of 10−12, likely to sustain of pyrrole-carboxylic acids, amidated with a short-chain amine. These species are again found in F2, but with a much lower intensity. This fraction shows a relative abundance of 6.0% and covers 329 species. The highest intensities are recognized at a DBE of 7−9 and a Cn from 13 to 16. These species are assumed to be indoles, derivatized amides, or other N-heteroaromatics, such as benzimidazoles with higher DBE substituted with methoxy groups.[55] A similar compositional space is identified in F4, which shows a relative abundance of 7.4% with 358 species. In addition, high intensity can be noted at a DBE of 2 and a Cn of 16, which is likely related to a nitrogenated aliphatic compound, but which has not been reported in hydrothermal conversion products so far. Fraction F3 shows 267 species in the O1N2 class at a significant relative abundance of 17.8%. The related species are again located in the aromatic area, with a broad intensity range between the DBE values of 6−10 and a Cn of 11−18. These species can be accounted for O-substituted pyridine-based structure or other strong basic N-containing compounds, such as aromatic branched amines.

The O2N1 class in F1 shows a relative abundance of 13.1% covering a range of 383 species. High intensities are sharply located at a DBE of 2 and a Cn of 16 and 18. These species can clearly be defined as long-chain aliphatics that originate from fatty acids, including a combination of carboxylic with amine groups or amide with a hydroxy group or a ketone group. Described species also appear in F2 and F4 with high intensities. These fractions show a relative abundance of 8.8 and 7.5%, including 344 and 356 species, respectively. In addition, increased intensities in F2 are identified in the aromatic region, especially at a DBE of 7 and a Cn of 13, likely including indole and carboxylic groups. In F4, the aromatic region shows increased intensities over a broad range. A maximum is located at a DBE of 3 and a Cn of 10, suggesting the presence of pyrroles, branched with methoxy or hydroxyl groups. Another maximum of intensities with wider distribution is identified at a DBE of 7 and 8, from a DBE of 14 to 16, allocating species including N-heteroaromatics identified in N1 class in combination with hydroxy, methoxy, carbonyl, or carboxyl branches. On the contrary, F3 does not show any aliphatic species within the detected 148 species of the O2N1 class. The plot represents a relative abundance of 3.2% with the highest intensity identified at a DBE of 7 and a Cn between 15 and 17. These species are assumed to consist of furopyridines and methoxy or hydroxyl substitutions or alkylated amines with benzene or a hydroxyl group branched. Comparing the relative abundances and compositional space of the O*x*N*x* classes of the biocrude and F4, only minor effects can be observed. For the O1N1 and O2N1 class, the space abundances are slightly increased, whereas the identified species are decreased. Otherwise, in the O1N2 class the relative abundance is decreased, as again a majority of these compounds accumulate in F3. The described structures of the O1N1, O1N2, and O2N1 classes are schematized in Figure 8.

O*x*-Classes. Qualitatively, the O-containing O1 and O2 classes are discussed briefly. Their relative intensity scatter plots are shown in Supporting Information, S4. As only low relative abundances of the O*x* species are found in fraction F3, only for F1, F2, and F4 plots are shown. Within the compositional space of the graphs, high intensities with a DBE of 0−3 and a Cn of 16−18 are identified, suggesting the presence of saturated and unsaturated fatty acids, as well as their decarboxylation and dehydration products such as fatty acid alcohols and ketones. In F4, increased intensities are noted in an area of higher DBE and low Cn space, which is likely to be identified as (poly)aromatics, branched by an aliphatic hydroxyl or a carbonyl group. Additionally, at a DBE of 5 and a Cn of 26, increased intensities are related to sterol derivatives. Phenols that are identified in F1 and F2 from GC−MS measurements are assumed to not be effectively ionized by APCI in the positive ion mode.[46]

Aromaticity of N-Containing Classes. The DBE to C (DBE/C) ratio was calculated to derive information about the corresponding aromaticity distribution of the 10 N-containing classes (N1, N2, N3, O1N1, O1N2, O1N3, O2N1, O2N2, O3N1, and O3N2) within the biocrude and extracted fractions F1 to F4. Previous studies on HTL biocrude fractions and pyrolysis oil samples demonstrated the usefulness of this method.[56,57] Ratios above a value of >0.7 can be assumed as aromatic species, whereas species above a value of >0.9 are poly-aromatic.[58] The ratios are displayed by violin plots in Figure 9. The kernel density plots are generated, by estimating and smoothing the frequency distribution of the DBE/C ratio. The inner boxplots identify the median value (white dot) and quartiles (black bar) and upper and lower whiskers (black line). The median is the value that lies exactly in the middle of data distribution. With the quartiles, the lowest and highest 25% frequencies are labeled. The whiskers define the minimum

https://doi.org/10.1021/acs.energyfuels.2c02622
Energy Fuels 2022, 36, 14292−14303

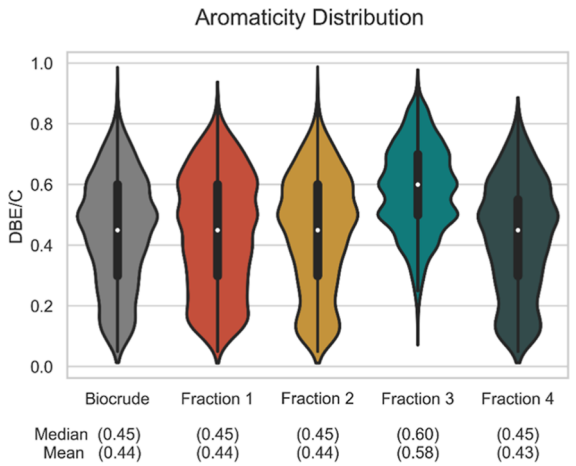

Figure 9. Violin plots of the aromatic distribution of N-containing compounds within the biocrude and the different fractions F1−F4. The distribution of the aromaticity (DBE/C) is represented as kernel density plots including boxplots. In addition, the median and mean values of the distribution are given.

and maximum values, showing possible outliers of the frequency distribution. In addition, the mean and the arithmetic average values are given.

The biocrude shows a kernel density curve with a peak at a value of 0.5 and median and mean values of 0.45 and 0.44, respectively. F1 shows an aromatic distribution up to a DBE/C value of 0.9 with a median at 0.45 and a mean at 0.44. The quartile bar ranges from 0.3 to 0.6 and the kernel density curve has a slight peak at a value of 0.6. In F2, the DBE/C distribution was found to show identical median and mean values, as well as that of the quartile bar. Peaks on the kernel density can be identified at DBE/C values of 0.1 and 0.5. Fraction F3 shows a divergent distribution pattern, with a peak around 0.5 and 0.6. The median and mean values in this fraction show the highest values of all fractions with 0.60 and 0.58, respectively. Furthermore, the quartile bar is assumed to be relatively narrow, reaching from 0.5 to 0.7. The kernel distribution plot of F4 shows almost the identical pattern as found for F2, with the same median value as for F1 and F2, but with a lower mean value at 0.43. In addition, fraction F4 shows the lowest upper quartile at 0.55, and with a lower quartile at 0.3, a narrow density distribution. The wide, uniform spread of species functionalized with an N-group in F1, can be related to the general low abundances within this fraction. F2 and F4 show local maxima in a lower range of DBE/C, according to the presence of aliphatic amide structures. Additionally, higher DBE/C ratios are related to the abundance of N-heteroaromatics such as previously identified pyrrole-based species (alkylated indole or carbazole derivates) which become more acidic with a higher degree of aromatization.[59] F3 shows a high aromatization degree with a relatively high mean value of the distribution. It is assumed that no nitrogenated aliphatic compounds are present in this fraction, only as a short side chain of aromatic species. The increased DBE/C values in this fraction can be referred to as multiple nitrogenated structures such as alkylated benzimidazoles or carbazolines.

CONCLUSIONS

The sequential extraction with two alkaline and one acidic aqueous solution could enrich complex and organic N-containing acids or bases in different extracts. Non-polar N-compounds remain within the residual fraction and are not able to be extracted by polar aqueous solutions. The mass balance and determination of the element content show significantly higher N- than C-recovery in the acid extracted fraction (F3). Nevertheless, the composition of the residual fraction (F4) remains quite complex, as a large share (50 wt % of N) of the N-compounds seems not to be extracted by aqueous basic or acidic solutions. In addition, the subsequent characterization of N-compounds of the biocrude at the molecular level was improved by the following. GC−MS resolution could be drastically increased, which led to improved identification of basic N-compounds and an association with FTICR MS to determine the structures of detected N-species. The results confirmed the presence of N-compounds in the acidic fraction (F3), as every identified compound is functionalized with N. The combination of the polar extraction methodology and the combination of GC−MS and FTICR MS analysis suggests that the basic N-functionalizations such as pyridinic-N are almost exclusively found in the acid extracted fraction (F3). Otherwise, a minor share of pyrrole and amide N-compounds is found in alkaline extracted fractions (F1 and F2). Most of the N-compounds found here are combined with a carboxylic acid group. Overall, these fractions resemble the residual F4, where N-compounds are found to be based on pyrrole and a large share consisting of amides. This is again reflected in the distribution of aromaticity of N-compounds over the fractions. Otherwise, the acidic extracted fraction shows a strong indication of the presence of N-heteroaromatics and no long-chain aliphatic structures.

Finally, with the gained knowledge a qualitative statement on the polarity behavior of N-compounds in HTL-biocrude from sewage sludge can be given. This is extremely important for the development of further downstream processes to a valuable fuel. The results suggest that N-heteroaromatics are strongly affected by the presence of polar groups. Eventually, the overall content of both heteroatoms and aromatic molecules must be reduced with a combination of suitable extraction, adsorption, or hydrotreating processes.

ASSOCIATED CONTENT

Supporting Information

The Supporting Information is available free of charge at https://pubs.acs.org/doi/10.1021/acs.energyfuels.2c02622.

Precipitate and emulsion formation; total-ion-current-chromatogram of GC−MS; identified compounds by GC−MS; Cn versus DBE plot of class O1-2; FTICR MS spectra; and spectral slices of O1N1 class (PDF)

AUTHOR INFORMATION

Corresponding Author

Klaus Raffelt − *Institute of Catalysis Research and Technology, Karlsruhe Institute of Technology, 76344 Eggenstein-Leopoldshafen, Germany;* orcid.org/0000-0001-5689-4443; Email: klaus.raffelt@kit.edu

Authors

Joscha Zimmermann − *Institute of Catalysis Research and Technology, Karlsruhe Institute of Technology, 76344 Eggenstein-Leopoldshafen, Germany;* orcid.org/0000-0001-6635-781X

Stefano Chiaberge − *Renewable, New Energies and Material Science Research Center Novara, 28100 Novara, Italy*

https://doi.org/10.1021/acs.energyfuels.2c02622
Energy Fuels 2022, 36, 14292−14303

Steen B. Iversen − *Steeper Energy, Hydrofaction Pilot and Test Facility, 9220 Aalborg Øst, Denmark*
Nicolaus Dahmen − *Institute of Catalysis Research and Technology, Karlsruhe Institute of Technology, 76344 Eggenstein-Leopoldshafen, Germany*

Complete contact information is available at: https://pubs.acs.org/10.1021/acs.energyfuels.2c02622

Author Contributions

The manuscript was written through contributions of all authors. All authors have given approval to the final version of the manuscript.

Funding

This project has received funding from the European Union's Horizon 2020 research and innovation programme under grant agreement no. 818413 (NextGenRoadFuel—Sustainable Drop-In Transport fuels from HTL of low value urban feedstocks).

Notes

The authors declare no competing financial interest.

■ ACKNOWLEDGMENTS

Konrad Völker [Institute of Catalysis and Technology Research (IKFT)] is acknowledged for his assistance in laboratory experiments.

■ REFERENCES

(1) Manara, P.; Zabaniotou, A. Towards Sewage Sludge Based Biofuels via Thermochemical Conversion − A Review. *Renewable Sustainable Energy Rev.* **2012**, *16*, 2566−2582.
(2) Fan, Y.; Fonseca, F. G.; Gong, M.; Hoffmann, A.; Hornung, U.; Dahmen, N. Energy Valorization of Integrating Lipid Extraction and Hydrothermal Liquefaction of Lipid-Extracted Sewage Sludge. *J. Cleaner Prod.* **2021**, *285*, 124895.
(3) Korving, L.; Van Loosdrecht, M.; Wilfert, P.Effect of Iron on Phosphate Recovery from Sewage Sludge. *Phosphorus Recovery and Recycling*; Springer Singapore: Singapore, 2019; pp 303−326.
(4) Eurostat. Sewage sludge production and disposal in the EU. http://appsso.eurostat.ec.europa.eu/nui/submitViewTableAction.do (accessed Aug 8, 2020).
(5) Hatinoğlu, M. D.; Sanin, F. D. Sewage Sludge as a Source of Microplastics in the Environment: A Review of Occurrence and Fate during Sludge Treatment. *J. Environ. Manage.* **2021**, *295*, 113028.
(6) Syed-Hassan, S. S. A.; Wang, Y.; Hu, S.; Su, S.; Xiang, J. Thermochemical Processing of Sewage Sludge to Energy and Fuel: Fundamentals, Challenges and Considerations. *Renewable Sustainable Energy Rev.* **2017**, *80*, 888−913.
(7) Verlicchi, P.; Zambello, E. Pharmaceuticals and Personal Care Products in Untreated and Treated Sewage Sludge: Occurrence and Environmental Risk in the Case of Application on Soil—A Critical Review. *Sci. Total Environ.* **2015**, *538*, 750−767.
(8) Castello, D.; Pedersen, T. H.; Rosendahl, L. A. Continuous Hydrothermal Liquefaction of Biomass: A Critical Review. *Energies* **2018**, *11*, 3165.
(9) Gollakota, A. R. K.; Kishore, N.; Gu, S. A Review on Hydrothermal Liquefaction of Biomass. *Renewable Sustainable Energy Rev.* **2018**, *81*, 1378−1392.
(10) Silva Thomsen, L. B.; Carvalho, P. N.; dos Passos, J. S.; Anastasakis, K.; Bester, K.; Biller, P. Hydrothermal Liquefaction of Sewage Sludge; Energy Considerations and Fate of Micropollutants during Pilot Scale Processing. *Water Res.* **2020**, *183*, 116101.
(11) Chand, R.; Sadetmahaleh, K. K.; Pedersen, T. H.; Toor, S.; Vollertsen, J.The Fate of Microplastics When Making Sludge into Crude Oil−the Impact of a Hydrothermal Liquefaction Process on Microplastics in Wastewater Treatment Plant Sludge. *MICRO 2020—Fate and Impacts of Microplastics: Knowledge and Responsibilities*, 2020.
(12) Fonts, I.; Gea, G.; Azuara, M.; Ábrego, J.; Arauzo, J. Sewage Sludge Pyrolysis for Liquid Production: A Review. *Renewable Sustainable Energy Rev.* **2012**, *16*, 2781−2805.
(13) Chacón-Parra, A.; Lewis, D.; van Eyk, P. The Effect of Ethanol as a Homogeneous Catalyst on the Reaction Kinetics of Hydrothermal Liquefaction of Lipids. *Chem. Eng. J.* **2021**, *414*, 128832.
(14) Madsen, R. B.; Zhang, H.; Biller, P.; Goldstein, A. H.; Glasius, M. Characterizing Semivolatile Organic Compounds of Biocrude from Hydrothermal Liquefaction of Biomass. *Energy Fuel.* **2017**, *31*, 4122−4134.
(15) Pedersen, T. H.; Rosendahl, L. A. Production of Fuel Range Oxygenates by Supercritical Hydrothermal Liquefaction of Lignocellulosic Model Systems. *Biomass Bioenergy* **2015**, *83*, 206−215.
(16) Panisko, E.; Wietsma, T.; Lemmon, T.; Albrecht, K.; Howe, D. Characterization of the Aqueous Fractions from Hydrotreatment and Hydrothermal Liquefaction of Lignocellulosic Feedstocks. *Biomass Bioenergy* **2015**, *74*, 162−171.
(17) Zhu, F.; Zhao, L.; Jiang, H.; Zhang, Z.; Xiong, Y.; Qi, J.; Wang, J. Comparison of the Lipid Content and Biodiesel Production from Municipal Sludge Using Three Extraction Methods. *Energy Fuel.* **2014**, *28*, 5277−5283.
(18) Zimmermann, J.; Raffelt, K.; Dahmen, N. Sequential Hydrothermal Processing of Sewage Sludge to Produce Low Nitrogen Biocrude. *Processes* **2021**, *9*, 491.
(19) Cheng, F.; Cui, Z.; Chen, L.; Jarvis, J.; Paz, N.; Schaub, T.; Nirmalakhandan, N.; Brewer, C. E. Hydrothermal Liquefaction of High- and Low-Lipid Algae: Bio-Crude Oil Chemistry. *Appl. Energy* **2017**, *206*, 278−292.
(20) Chiaberge, S.; Leonardis, I.; Fiorani, T.; Bianchi, G.; Cesti, P.; Bosetti, A.; Crucianelli, M.; Reale, S.; De Angelis, F. Amides in Bio-Oil by Hydrothermal Liquefaction of Organic Wastes: A Mass Spectrometric Study of the Thermochemical Reaction Products of Binary Mixtures of Amino Acids and Fatty Acids. *Energy Fuel.* **2013**, *27*, 5287−5297.
(21) Fan, Y.; Hornung, U.; Dahmen, N.; Kruse, A. Hydrothermal Liquefaction of Protein-Containing Biomass: Study of Model Compounds for Maillard Reactions. *Biomass Convers. Biorefin.* **2018**, *8*, 909−923.
(22) Elliott, D. C.; Hart, T. R.; Neuenschwander, G. G.; Rotness, L. J.; Roesijadi, G.; Zacher, A. H.; Magnuson, J. K. Hydrothermal Processing of Macroalgal Feedstocks in Continuous-Flow Reactors. *ACS Sustainable Chem. Eng.* **2014**, *2*, 207.
(23) Castello, D.; Haider, M. S.; Rosendahl, L. A. Catalytic Upgrading of Hydrothermal Liquefaction Biocrudes: Different Challenges for Different Feedstocks. *Renewable Energy* **2019**, *141*, 420−430.
(24) Furimsky, E.; Massoth, F. E. Hydrodenitrogenation of Petroleum. *Catal. Rev.* **2005**, *47*, 297−489.
(25) Prado, G. H. C.; de Klerk, A. Metals Removal from Metal-Bridged Molecules by Acid Treatment of Oilsands Bitumen and Subfractions. *Energy Fuel.* **2016**, *30*, 20−30.
(26) Jarvis, J. M.; Sudasinghe, N. M.; Albrecht, K. O.; Schmidt, A. J.; Hallen, R. T.; Anderson, D. B.; Billing, J. M.; Schaub, T. M. Impact of Iron Porphyrin Complexes When Hydroprocessing Algal HTL Biocrude. *Fuel* **2016**, *182*, 411−418.
(27) Furimsky, E.; Massoth, F. E. Deactivation of Hydroprocessing Catalysts. *Catal. Today* **1999**, *52*, 381−495.
(28) Haider, M. S.; Castello, D.; Rosendahl, L. A. The Art of Smooth Continuous Hydroprocessing of Biocrudes Obtained from Hydrothermal Liquefaction: Hydrodemetallization and Propensity for Coke Formation. *Energy Fuel.* **2021**, *35*, 10611−10622.
(29) Li, H.; Zhu, Z.; Lu, J.; Watson, J.; Kong, D.; Wang, K.; Zhang, Y.; Liu, Z. Establishment and Performance of a Plug-Flow Continuous Hydrothermal Reactor for Biocrude Oil Production. *Fuel* **2020**, *280*, 118605.
(30) Wu, H.; Li, H.; Fang, Z. Hydrothermal Amination of Biomass to Nitrogenous Chemicals. *Green Chem.* **2021**, *23*, 6675−6697.

(31) Ekpo, U.; Ross, A. B.; Camargo-Valero, M. A.; Fletcher, L. A. Influence of PH on Hydrothermal Treatment of Swine Manure: Impact on Extraction of Nitrogen and Phosphorus in Process Water. *Bioresour. Technol.* **2016**, *214*, 637−644.
(32) Chen, W. T.; Tang, L.; Qian, W.; Scheppe, K.; Nair, K.; Wu, Z.; Gai, C.; Zhang, P.; Zhang, Y. Extract Nitrogen-Containing Compounds in Biocrude Oil Converted from Wet Biowaste via Hydrothermal Liquefaction. *ACS Sustainable Chem. Eng.* **2016**, *4*, 2182−2190.
(33) Fonts, I.; Navarro-Puyuelo, A.; Ruiz-Gómez, N.; Atienza-Martínez, M.; Wisniewski, A.; Gea, G. Assessment of the Production of Value-Added Chemical Compounds from Sewage Sludge Pyrolysis Liquids. *Energy Technol.* **2017**, *5*, 151−171.
(34) Jarvis, J. M.; Albrecht, K. O.; Billing, J. M.; Schmidt, A. J.; Hallen, R. T.; Schaub, T. M. Assessment of Hydrotreatment for Hydrothermal Liquefaction Biocrudes from Sewage Sludge, Microalgae, and Pine Feedstocks. *Energy Fuel.* **2018**, *32*, 8483−8493.
(35) Kazi, Z. H.; Schnitzer, M. I.; Monreal, C. M.; Mayer, P. Separation and Identification of Heterocyclic Nitrogen Compounds in Biooil Derived by Fast Pyrolysis of Chicken Manure. *J. Environ. Sci. Health, Part B* **2010**, *46*, 51−61.
(36) Torri, C.; Garcia Alba, L.; Samorì, C.; Fabbri, D.; Brilman, D. W. F. Hydrothermal Treatment (HTT) of Microalgae: Detailed Molecular Characterization of HTT Oil in View of HTT Mechanism Elucidation. *Energy Fuel.* **2012**, *26*, 658−671.
(37) Han, J.; Li, X.; Kong, S.; Xian, G.; Li, H.; Li, X.; Li, J.; Zhang, J.; Meng, H.; Wang, H.; et al. Characterization of Column Chromatography Separated Bio-Oil Obtained from Hydrothermal Liquefaction of Spirulina. *Fuel* **2021**, *297*, 120695.
(38) Boocock, D. G. B.; Kallury, R. K. M. R.; Tidwell, T. T. Analysis of Oil Fractions Derived from Hydrogenation of Aspen Wood. *Anal. Chem.* **1983**, *55*, 1689−1694.
(39) Dote, Y.; Ogi, T.; Yokoyama, S.; Minowa, T.; Sawayama, S.; Hayashi, T.; Suzuki, A.Analysis of Oil Derived from Liquefaction of Sewage Sludge. In *Advances in Thermochemical Biomass Conversion*; Bridgwater, A. V., Ed.; Springer Netherlands: Dordrecht, 1993; pp 1378−1384.
(40) Das, D. D.; Schnitzer, M. I.; Monreal, C. M.; Mayer, P. Chemical Composition of Acid−Base Fractions Separated from Biooil Derived by Fast Pyrolysis of Chicken Manure. *Bioresour. Technol.* **2009**, *100*, 6524−6532.
(41) Kozhinov, A. N.; Zhurov, K. O.; Tsybin, Y. O. Iterative Method for Mass Spectra Recalibration via Empirical Estimation of the Mass Calibration Function for Fourier Transform Mass Spectrometry-Based Petroleomics. *Anal. Chem.* **2013**, *85*, 6437−6445.
(42) ChemSpider Database. http://www.chemspider.com/ (accessed Nov 25, 2021).
(43) Haider, M. S.; Castello, D.; Rosendahl, L. A. Two-stage catalytic hydrotreatment of highly nitrogenous biocrude from continuous hydrothermal liquefaction: A rational design of the stabilization stage. *Biomass and Bioenergy* **2020**, *139*, 105658.
(44) Speight, J. G.*The Chemistry and Technology of Petroleum*; CRC Press, 2014.
(45) Chiaberge, S.; Siviero, A.; Passerini, C.; Pavoni, S.; Bianchi, D.; Haider, M. S.; Castello, D. Co-Processing of Hydrothermal Liquefaction Sewage Sludge Biocrude with a Fossil Crude Oil by Codistillation: A Detailed Characterization Study by FTICR Mass Spectrometry. *Energy Fuel.* **2021**, *35*, 13830−13839.
(46) Huba, A. K.; Huba, K.; Gardinali, P. R. Understanding the Atmospheric Pressure Ionization of Petroleum Components: The Effects of Size, Structure, and Presence of Heteroatoms. *Sci. Total Environ.* **2016**, *568*, 1018−1025.
(47) Simoneit, B. R. T.; Rushdi, A. I.; bin Abas, M. R. B.; Didyk, B. M. Alkyl Amides and Nitriles as Novel Tracers for Biomass Burning. *Environ. Sci. Technol.* **2003**, *37*, 16−21.
(48) Jarvis, J. M.; Billing, J. M.; Hallen, R. T.; Schmidt, A. J.; Schaub, T. M. Hydrothermal Liquefaction Biocrude Compositions Compared to Petroleum Crude and Shale Oil. *Energy Fuel.* **2017**, *31*, 2896−2906.
(49) Kazi, Z. H.; Schnitzer, M. I.; Monreal, C. M.; Mayer, P. Separation and identification of heterocyclic nitrogen compounds in biooil derived by fast pyrolysis of chicken manure. *J. Environ. Sci. & Health, Part B* **2010**, *46*, 51−61.
(50) Cao, J.-P.; Zhao, X.-Y.; Morishita, K.; Wei, X.-Y.; Takarada, T. Fractionation and identification of organic nitrogen species from bio-oil produced by fast pyrolysis of sewage sludge. *Bioresource Technology* **2010**, *101* (19), 7648−7652.
(51) Walba, H.; Ruiz-Velasco, R. LFER [Linear Free Energy Relations] for Amphoteric 5- (or 6-)Substituted Benzimidazoles. *J. Org. Chem.* **1969**, *34*, 3315−3320.
(52) Sudasinghe, N.; Dungan, B.; Lammers, P.; Albrecht, K.; Elliott, D.; Hallen, R.; Schaub, T. High Resolution FT-ICR Mass Spectral Analysis of Bio-Oil and Residual Water Soluble Organics Produced by Hydrothermal Liquefaction of the Marine Microalga Nannochloropsis Salina. *Fuel* **2014**, *119*, 47−56.
(53) Murata, M. Browning and Pigmentation in Food through the Maillard Reaction. *Glycoconjugate J.* **2021**, *38*, 283−292.
(54) He, L.; Ma, Y.; Yue, C.; Wu, J.; Li, S.; Wang, Q.; Wang, B. Transformation Mechanisms of Organic S/N/O Compounds during Microwave Pyrolysis of Oil Shale: A Comparative Research with Conventional Pyrolysis. *Fuel Process. Technol.* **2021**, *212*, 106605.
(55) Torri, C.; Garcia Alba, L.; Samorì, C.; Fabbri, D.; Brilman, D. W. F. Hydrothermal Treatment (HTT) of Microalgae: Detailed Molecular Characterization of HTT Oil in View of HTT Mechanism Elucidation. *Energy Fuel.* **2012**, *26*, 658−671.
(56) Gaspar, A.; Zellermann, E.; Lababidi, S.; Reece, J.; Schrader, W. Characterization of Saturates, Aromatics, Resins, and Asphaltenes Heavy Crude Oil Fractions by Atmospheric Pressure Laser Ionization Fourier Transform Ion Cyclotron Resonance Mass Spectrometry. *Energy Fuel.* **2012**, *26*, 3481−3487.
(57) Xu, Y.; Schrader, W. Studying the Complexity of Biomass Derived Biofuels. *Energies* **2021**, *14*, 2032.
(58) Santos, J. M.; Vetere, A.; Wisniewski, A.; Eberlin, M. N.; Schrader, W. Modified SARA Method to Unravel the Complexity of Resin Fraction(s) in Crude Oil. *Energy Fuel.* **2020**, *34*, 16006−16013.
(59) Bordwell, F. G.; Drucker, G. E.; Fried, H. E. Acidities of Carbon and Nitrogen Acids: The Aromaticity of the Cyclopentadienyl Anion. *J. Org. Chem.* **1981**, *46*, 632−635.

https://doi.org/10.1021/acs.energyfuels.2c02622
Energy Fuels 2022, 36, 14292−14303